Photoelectron Spectroscopy of the Trimethylenemethane Negative Ion

Paul G. Wenthold
Department of Chemistry and Biochemistry, Texas Tech University, Lubbock, Texas, USA

Jun Hu* and Robert R. Squires
Department of Chemistry, Purdue University, West Lafayette, Indiana, USA

W. Carl Lineberger
JILA, University of Colorado and National Institute of Standards and Technology, and Department of Chemistry and Biochemistry, University of Colorado, Boulder, Colorado, USA

The photoelectron spectrum of the trimethylenemethane (TMM) negative ion is described. The electron affinity of TMM is found from the spectrum to be 0.431 ± 0.006 eV, and the energy difference between the $\tilde{X}\ ^3A_2'$ and $\tilde{b}\ ^1A_1$ states of TMM is determined to be 16.1 ± 0.2 kcal/mol. The energy difference between the lowest energy triplet and singlet states is estimated to be 13–16 kcal/mol. The enthalpy of formation of TMM is measured to be 70 ± 3 kcal/mol, and the C–H bond enthalpy in 2-methylallyl radical is 90 ± 2 kcal/mol. Previously unobserved vibrational frequencies of 425, 915, and 1310 cm^{-1} are found for the triplet state of TMM, whereas a frequency of 325 cm^{-1} is found for the singlet state. In addition, an overtone peak is observed for the triplet state at 1455 cm^{-1}, and both states contain peaks that are assigned to bands arising from excited vibrational levels of the ion. (J Am Soc Mass Spectrom 1999, 10, 800–809) © 1999 American Society for Mass Spectrometry

An important application of mass spectrometry that has emerged in recent years is in the field of physical organic chemistry, and the study of organic reactive intermediates. Among the most useful properties that can be obtained directly from mass spectrometry studies are thermochemical data, including proton affinities, gas-phase acidities, ionization potentials, and electron affinities. In addition, these quantities can be used to derive others, such as bond dissociation energies and enthalpies of formation. These capabilities are probably best illustrated by the measurements of the enthalpy of formation of *o*-benzyne. In the past 20 years, there have been at least eight independent measurements of the enthalpy of formation of *o*-benzyne, involving at least seven different gas-phase ion methods [1–8]. The internal consistency of the results obtained from completely independent approaches provides a solid measurement of this important thermochemical property.

In the past decade, we have been using negative ion photoelectron spectroscopy to investigate the properties of highly reactive organic intermediates, including radicals [9–13], carbenes [10, 14–20], biradicals [21–23], strained ring systems [24], and even reaction transition states [25]. From these studies, we obtain not only thermochemical properties such as those described above but also spectroscopic information for these species, providing a more detailed understanding of their structure and bonding.

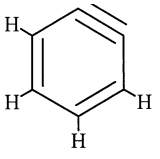

o-Benzyne

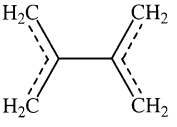

TME

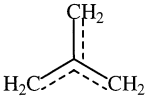

TMM

More importantly, negative ion photoelectron spectroscopy studies can be used to address controversial issues that have appeared in the field of physical organic chemistry. For example, the identity of the ground state of tetramethyleneethene (TME) biradical has provoked heated debate over the recent years. Experimental studies suggest a triplet ground state for TME [26–28], while theory favors the singlet state [29–36]. Additional insight to the problem was obtained recently from the photoelectron spectrum of the TME negative ion [37]. The intensities of the singlet and

Address reprint requests to Dr. Paul G. Wenthold, Department of Chemistry and Biochemistry, MS 1061, Texas Tech University, Lubbock, TX 79409-1061. E-mail: qepgw@ttu.edu

* Current address: Department of Chemistry, North Carolina State University, Raleigh, NC 27695.

Dedicated to the memory of Professor Robert Squires.

1044-0305/99/$20.00
PII S1044-0305(99)00043-4

Received December 2, 1998
Revised February 18, 1999
Accepted February 22, 1999

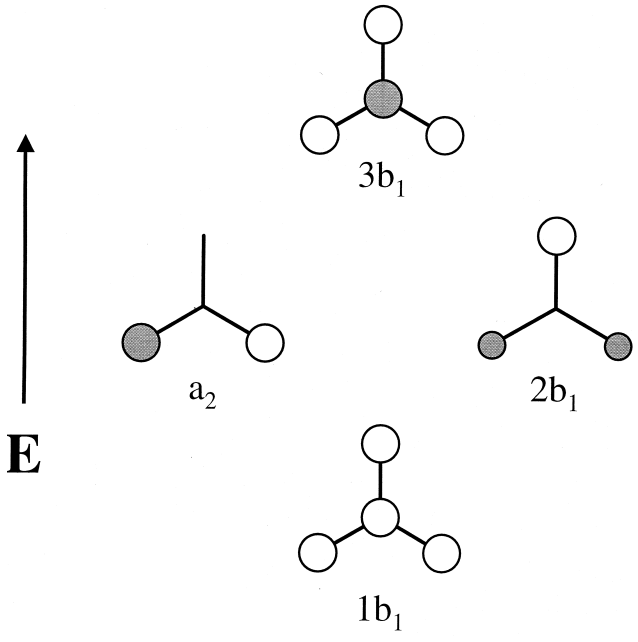

Figure 1. The π molecular orbitals of trimethylenemethane. Symmetry labels refer to the C_{2v} molecule.

triplet features were used to assign the singlet as the ground state, with the triplet state 2–3 kcal/mol higher in energy. Therefore, the photoelectron measurements confirmed the prediction of a singlet ground state for the gas-phase molecule.

Recently, we reported [38] the photoelectron spectrum of the negative ion of trimethylenemethane (TMM), another notorious biradical [39–42]. Originally recognized by Moffitt and Coulson 50 years ago [43], this non-Kekulé molecule has since inspired numerous computational studies involving a wide variety of theoretical methods. Although trimethylenemethanes were commonly invoked as intermediates in the formation and rearrangement of methylenecyclopropanes [44, 45], they are also fundamentally important because they serve as a paradigm for basic theoretical concepts such as free valence, disjoint orbital analysis, and negative spin-density in π systems [46]. Little was known experimentally about TMM until 1966, when Dowd [47] reported the EPR spectrum for TMM isolated in a glassy matrix at 88 K. Subsequent work on TMM [39, 48–50] and monocyclic derivatives [40, 51] has lead to an in-depth understanding of their electron structure and chemical reactivity. Recently, the infrared spectra of TMM and deuterated isotopomers were reported [52, 53], providing the first vibrational data for the biradical. Practical applications of TMM derivatives have also been developed, and include organic ferromagnets [54], synthetic reagents [55], and even DNA cleaving agents [56].

The electronic structure of TMM is well established [46]. The π molecular orbitals in planar TMM are shown in Figure 1. Occupation of these orbitals gives rise to a $^3A_2'$ state with D_{3h} symmetry, and a $^1E'$ state, which undergoes a second-order Jahn–Teller distortion to give two singlets, $^1A_1$ and $^1B_2$, with C_{2v} geometries. Borden and Davidson [57] have shown that the $^1B_2$ state is actually a transition state for the pseudorotation of the $^1A_1$ state. Moreover, Davis and Goddard have shown that the $^1B_2$ state is unstable with respect to rotation of one of the methylene units to form a stable, nonplanar $^1B_1$ state. Therefore, the $^1B_2$ state of TMM is a maximum in two coordinates on the potential energy surface (a "mountain top").

For the most part, previous computational studies have not addressed the nature of the $^1A_1$ state [58–61], although Feller et al. did note that the region of the potential energy surface around the $^1A_1$ is relatively flat [62]. Recent frequency calculations [63] at the MCSCF(4,4)/6 − 31G* level of theory actually suggest that $^1A_1$ TMM is a saddle point that connects two equivalent C_2 states. Each C_2 state is a transition state that exchanges the out-of-plane methylene with a planar methylene in the $^1B_1$ state. However, the imaginary frequency at this level of theory is only 70*i*. In fact, at the MCSCF(4,4)/6 − 31 + G* level of theory the frequency for the same mode is real, indicating that the $^1A_1$ state is a true minimum [38]. At the highest levels of theory, the $^1B_1$ state is calculated to be 0–3 kcal/mol lower in energy than the $^1A_1$ state, which is destabilized by electron repulsion [57]. Although the $^1B_2$ is generally calculated to be comparable in energy to the $^1A_1$ state, the fact that it is a mountain top means that it likely would not be observed in the photoelectron spectrum.

The energy difference between the singlet and triplet states of TMM (the "singlet-triplet splitting") has been of considerable interest. Early computational studies predicted the energy difference between the $^3A_2'$ and $^1B_1$ states to be 15–20 kcal/mol [58–62, 64–67]. An experimental estimate of ~7 kcal/mol was provided by Dowd and Chow [68], who measured the temperature dependence of the rate of disappearance of the EPR signal for the matrix isolated triplet biradical. If it is assumed that the rate determining step for the signal loss is intersystem crossing, then the measured activation energy can be equated with the singlet–triplet splitting. The value reported by Dowd and Chow is significantly lower than that predicted by the theoretical studies [58, 60, 61, 64–66], and is lower than the predicted barrier for the

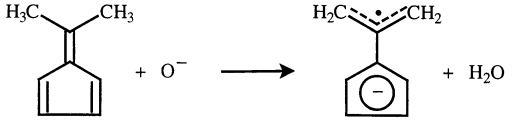

(1)

ring closure [59, 62, 67, 69, 70].

In order to study the properties of TMM using negative ion photoelectron spectroscopy, it is necessary to be able to generate the ion in the gas phase. A common method of making ions of biradicals is to use

the reaction of hydrocarbons with the atomic oxygen ion, O^- [71]. This approach has been used to generate the ions of biradicals similar to TMM, including *m*-xylylene [72] and tetramethyleneethene [71]. For example, the reaction of dimethylfulvene with O^- has been used recently [73] to prepare the negative ion of cyclopentadienylidenetrimethylenemethane (eq 1), a famous derivative of TMM [40, 51]. Unfortunately, this approach does not work for the negative ion of TMM, as the reaction of O^- with isobutene proceeds mainly by hydrogen atom transfer [71]. The synthesis of the negative ion of TMM can be accomplished using the method developed by Squires and co-workers [74] involving the reaction of 2-trimethylsilylmethylallyl anion with molecular fluorine, F_2 (eq 2) [75]. The TMM structure of the ion was verified by reactions with nitric oxide (NO) and nitrous oxide (N_2O), which showed that the ion was allylic and contained three equivalent methylene groups [38].

In this article, we give a complete account of our negative ion photoelectron spectroscopy studies of TMM. The negative ion was generated using the procedure shown in eq 2. Molecular orbital calculations on the electronic structure of the molecular ion are described and utilized in the analysis of the spectrum. In addition to describing our measurements of the singlet–

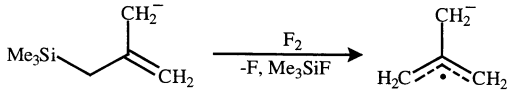

(2)

triplet splitting, we discuss the rich vibrational structure observed in the photoelectron spectrum, and propose assignments of vibrational frequencies in both the singlet and triplet states of TMM.

Experimental

The photoelectron spectrometer and experimental procedures have been described in detail previously [76], and only a summary is provided here. Primary reactant ions are generated in the flowing afterglow source for the photoelectron spectrometer by adding a gaseous mixture of the neutral precursor and helium (0.5 torr) into the plasma produced by a microwave discharge. Subsequent ion/molecule reactions between primary ions and neutral reagents gases added through ring inlets downstream in the flow tube can be used to carry out ion synthesis. In this work, the negative ion of TMM was prepared by first adding vapors of the *bis*-trimethylsilyl precursor immediately downstream from the microwave discharge. An ion with a mass-to-charge ratio and photoelectron spectrum consistent with that expected for 2-trimethylsilylmethylallyl anion was observed under these conditions, presumably formed by plasma ionization. The TMM ion is formed by adding F_2 (5% in He) farther downstream. It is possible to cool the ions to subambient temperatures by immersing the flowing afterglow in liquid nitrogen. Spectra for TMM^- were recorded for ions formed at both room temperature and with liquid nitrogen cooling, but all the spectra reported here are for cooled ions. A small portion of the ions is extracted through a 1-mm orifice in a nosecone into a differentially pumped chamber, where they are focused, accelerated to 735 eV, mass selected with a Wien velocity filter ($M/\Delta M \approx 40$), and then decelerated to 40 eV prior to entering the laser interaction region. The ion beam is crossed with the 351-nm output of an argon ion laser in a buildup cavity as described previously. Photodetached electrons are energy analyzed with ~8 meV resolution by a hemispherical analyzer, and detected using position-sensitive detection. The photoelectron spectrum depicts the number of electrons detected as a function of electron binding energy, which is given by the difference between the laser photon energy (3.531 19 eV) and the electron kinetic energy.

The absolute energy scale is calibrated by the position of the $^3P_2 + e^- \leftarrow {}^2P_{3/2}$ peak in the spectrum of O^- [EA(O) = 1.461 12 eV] [77], which is formed by microwave discharge on O_2. A small energy scale compression factor is determined by comparing the measured relative peak positions in the spectrum of tungsten ion with the known term energies of tungsten atom [78]. The extent of the scale compression is less than 1%, and absolute photoelectron energies can be obtained to an accuracy of ±0.003 meV.

Proton affinity measurements were made using the flowing afterglow–triple quadrupole instrument at Purdue. The apparatus and experimental procedures have been described previously [79]. In the present experiments, TMM^- ions created in the flow tube were extracted through a 1-mm orifice in a nose cone into an EXTREL triple quadrupole mass analyzer. For energy resolved mass spectra, the TMM^- reactant ion was selected using the first quadrupole and injected into the second quadrupole, which is a gas-tight reaction cell containing neutral reagent gas at a pressure of ~0.05 mtorr to minimize the occurrence of secondary collisions. The product ions were mass analyzed using the third quadrupole and detected with an electron multiplier operating in pulse counting mode. The intensity of the product ion was monitored as a function of the axial kinetic energy of the reactant ions, determined by the quadrupole dc offset voltage. The center-of-mass (c.m.) collision energy is calculated from the expression $E_{c.m.} = E_{lab}[m/(m + M)]$, where E_{lab} is the axial kinetic energy in the lab frame, m is the mass of the reactant ion, and M is the mass of the neutral target.

A plot of the product ion yield versus the center-of-mass collision energy gives an appearance curve from which the activation energy for the reaction can be obtained. The product ion appearance curve is fitted with an assumed model function (eq 3) [80],

$$\sigma(E) = \sigma_0 \sum g_i(E + E_i - E_T)^n/E \quad (3)$$

where $\sigma(E)$ is the relative cross section at the center-of-mass collision energy, E, E_T is the reaction threshold, σ_0 is a scaling parameter, and n is an adjustable parameter. The vibrational energies of the ionic and neutral reactants (E_i) are also added explicitly into the fit. Data analysis is carried out utilizing the CRUNCH program written by Armentrout and co-workers, which optimizes the fit using an iterative procedure in which the parameters σ_0, E_T, and n are varied so to minimize the deviation between the model and the steeply rising portion of the appearance curve. Convoluted into the fit are the reactant ion kinetic energy distribution, approximated by a Gaussian function with a 1.5-eV (lab) FWHM, and a Doppler broadening function [81] to account for the random thermal motion of the neutral gas. The thresholds derived using this procedure correspond to the 0-K activation energies. These can be converted to the 298-K reaction enthalpies by adding the difference in the integrated heat capacities between the reactants and the products from 0 to 298 K. For the present study, it is expected that this difference is small, and it is assumed that $\Delta H_{298} = E_T$.

Materials

All reagents were purchased from commercial suppliers and were used as received. Fluorine, 5% in He, was purchased from Spectra. The *bis*-trimethylsilylisobutene precursor was prepared by quenching the corresponding dianion with chlorotrimethylsilane.

Structure of the Negative Ion

Before discussing the photoelectron spectrum of TMM^-, it is important to establish the structure of the negative ion. As discussed previously by Nash and Squires [82], negative ions of biradicals have two low-lying electronic states. For TMM, the two planar electronic states are the $^2A_2$ and $^2B_1$ states, which are formed by adding an electron to the b_1 and a_2 orbitals in triplet TMM, respectively (Figure 1). The $^2A_2$ state, with two electrons in the b_1 orbital and one electron in the A_2 orbital, is best described as consisting of an allyl radical with a methyl anion substituent, while the $^2B_1$ state consists of an allyl anion with a methyl radical substituent. The geometries, energies, and frequencies for the two electronic states were calculated at the B3LYP/aug-cc-pVDZ level of theory, and the calculated geometries are shown in Figure 2. Both ions adopt Jahn–Teller distorted, C_{2v} geometries that reflect the features expected given the electronic structures described above. The $^2B_1$ ion has a long carbon–carbon bond that attaches a methylene to the node of an allyl group. The carbon–carbon bond length to the methylene unit is 1.442 Å, and the carbon–carbon bonds in the allylic portion are 1.419 Å. The angle of the carbon atoms in the allylic portion is 126.9 °. The relative carbon–carbon bond lengths are inverted in the $^2A_2$ state, with the allylic bonds longer than the bond to the methylene group. The angle of the allyl portion is smaller for the $^2A_2$ state.

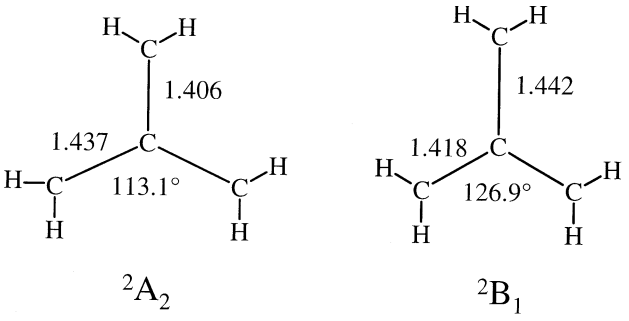

Figure 2. Calculated bond lengths and bond angles for the $^2A_2$ and $^2B_1$ states of the trimethylenemethane negative ion. Bond lengths are in angstroms, and bond angles are in degrees.

The frequencies calculated for the planar electronic states are listed in Table 1. All the frequencies for the $^2A_2$ state are real at this level of theory, indicating a true minimum on the potential energy surface. The $^2B_1$ state has a single imaginary frequency, and therefore is

Table 1. Properties of the $^2A_2$ and $^2B_1$ states of the TMM negative ion calculated at the B3LYP/aug-cc-pVDZ level of theory[a]

	$^2A_2$	$^2B_1$
Electronic energies, Hartrees	−155.96006	−155.95953
Vibrational frequencies, cm^{-1}		
a_1	451.0	431.7
	919.1	920.0
	1012.1	1002.5
	1374.3	1303.3
	1470.5	1450.9
	1493.3	1469.0
	3111.1	3111.4
	3123.8	3124.6
	3214.5	3202.8
a_2	307.3	233.2
	524.1	393.9
	620.4	439.9
b_1	314.0	406.9
	356.6	514.3
	661.9	606.9
b_2	279.6	532.1i
	935.9	937.2
	994.4	997.6
	1222.6	1085.3
	1438.9	1429.5
	3113.2	3112.3
	3192.6	3198.9
	3209.1	3210.8

[a]At the optimized geometries shown in Figure 2.

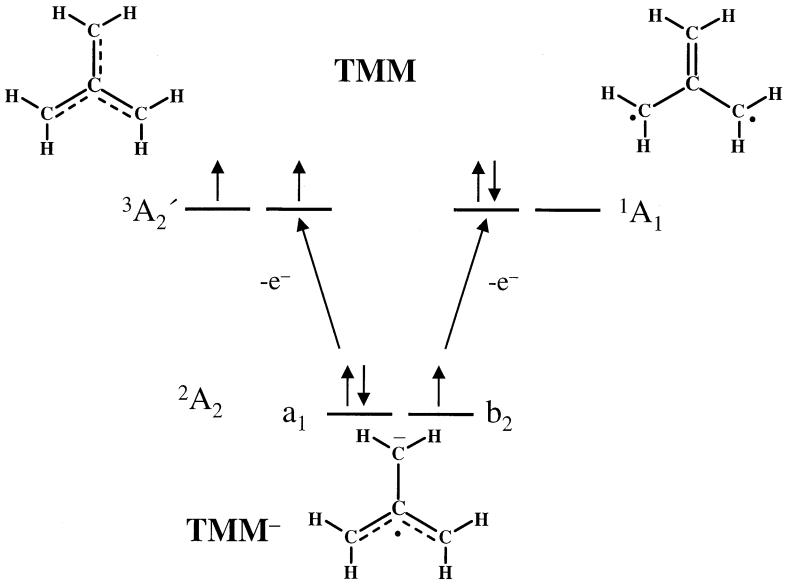

Figure 3. Expected photodetachment processes anticipated for the detachment of the $^2A_2$ state of the TMM negative ion. The same products would be expected to be formed upon detachment of the $^2B_2$ state.

calculated to be a saddle point on the potential energy surface. The difference in the electronic energies between the $^2A_2$ and the $^2B_1$ states of the ion is 0.3 kcal/mol. These results suggest that the $^2A_2$ ion is the ground state of the system, and that the $^2B_1$ state is a saddle point slightly higher in energy, although the difference is too small to make any definitive conclusions. Nonplanar electronic states of the ion were investigated but found to be much higher in energy (>10 kcal/mol) than the planar states. Therefore, we conclude that the ion is likely planar.

Regardless of whether the ground state of the ion is $^2A''$ or $^2B_1$, photodetachment should lead to formation to two planar electronic states, one singlet and one triplet (Figure 3). Given the large difference in the geometries of the ion and the $^1B_1$ states, detachment to form that state would be expected to be weak, if it occurs at all. Finally, vibrational activity is expected for formation of the triplet ground state, with the active mode being the Jahn–Teller coordinate that connects the C_{2v} ion to the D_{3h} triplet. The photoelectron spectrum of TMM^-, shown in Figure 4, conforms to these expectations.

Experimental Results

In this section, we provide a detailed description of the features observed in Figure 4. In the spectrum, two electronic states are observed, with the origin of the band corresponding to the lower energy state ~6 times more intense than that of the excited state. The ground state is readily assigned to the $\tilde{X}\ ^3A_2'$ state of TMM. An expanded view of this region is shown in Figure 5. The origin peak for this region (peak A) is at an electron binding energy of 0.431 ± 0.010 eV, the electron affinity of TMM. The positions of the remaining peaks (A–G) are listed at the top of Table 2. These peaks indicate at least four vibrational progressions of 200, 425, 1310, and 1455 cm^{-1}. Assignments of the vibrational modes are provided in a later section. A summary of the physical properties obtained for triplet TMM is given in Table 3.

The vibrational progressions observed in the spectrum result from differences between the geometries of the ion and the neutral. The extent of the geometry differences is indicated by the normal mode displacements, ΔQ_i, in mass-weighted Cartesian coordinates for the transition, which are the elements of the Duschinsky **K** matrix [83]. The displacements are obtained by fitting the experimental data using a procedure that is described elsewhere [76]. The largest normal coordinate displacement corresponds to the mode with a frequency of 425 cm^{-1}. The calculated fit to the triplet region is shown as a solid line in Figure 6, while the experimental data are shown as solid points. In order to obtain an

Table 2. Positions of peaks observed in the triplet region of the photoelectron spectrum of trimethylenemethane negative ion[a]

Peak label	Relative position	Peak label	Relative position
A	−505		
A	0	F	1040
B	200	G	1305
C	425	H	1460
D	615	I	1750
E	850	J	1920

[a]Relative positions in cm^{-1}. The origin peak is at 0.431 ± 0.006 eV.

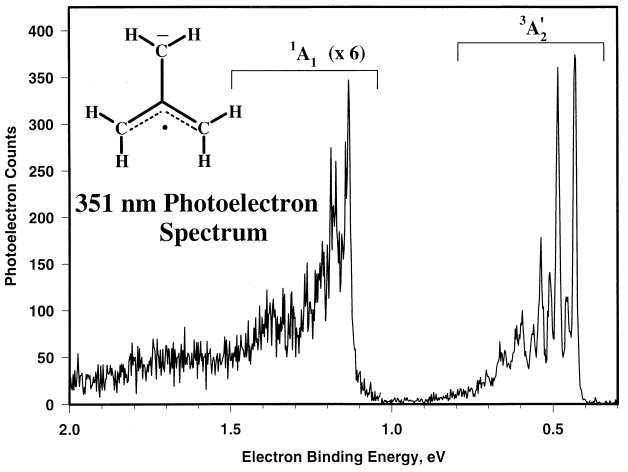

Figure 4. The 351-nm photoelectron spectrum of the TMM negative ion. The two features correspond to formation of the $^3A_2'$ and $^1A_1$ states of TMM.

Table 3. Measured properties of trimethylenemethane

	triplet, $^2A_2$	singlet, $^1A_1$
Electron binding energy, eV	0431 ± 0.006[a]	1.131 ± 0.006
Relative term energy, kcal/mol	0.0	16.1 ± 0.2
Vib freq,[b] cm^{-1} (ΔQ_i)[c]		
CCC bending	425 (0.336)	325
Sym CCC stretch[d]	915 (0.113)	
CC stretch	1310 (0.063)	
CH_2 twist overtone	1455 (0.071)	
Sequence band[e]	200 (0.182)	90
Ion CCC bending[f]	505	

[a]Corresponds to the electron affinity of TMM.
[b]Obtained from average peak spacings; see Table 2. Estimated uncertainty is 5%.
[c]The values in parentheses are normal coordinate displacements, in $amu^{1/2}$ Å.
[d]Obtained from a fit of the experimental data.
[e]Assigned to a band resulting from a transition from $v = 1$ in the ion to $v = 1$ in the neutral. See text for details.
[f]Determined from the position of the hot band.

accurate fit of the data, it was necessary to add an additional vibrational mode, with a frequency of 925 cm^{-1} and $\Delta Q_i = 0.10$ units. This frequency is included in the data in Table 3. A hot band observed in the spectrum (peak a) gives a frequency of 400 cm^{-1} for the ion.

The feature corresponding to formation of the higher energy state is significantly more congested than that for the ground state, and only four peaks are identified. The origin peak is found at 1.130 ± 0.006 eV, 0.699 ± 0.006 eV (16.1 ± 0.1 kcal/mol) higher in energy than the ground state. The remaining peaks are 85, 325, and 420 cm^{-1} higher in energy and indicate vibrational progressions of 90 and 325 cm^{-1}, respectively. The fact that the feature has a sharp, intense origin peak indicates that the geometry of the neutral is similar to that of the ion, and that the neutral is stable. As noted above, the feature for formation of the $^1B_1$ state would have a weak origin peak and an extended vibrational progression, while formation of the $^1B_2$ state would result in a significantly broadened peak [25, 84]. Therefore, we assign this feature to the planar, $\tilde{b}$ $^1A_1$ state of TMM. Although it has been suggested that the $^1A_1$ state is a transition state [63], we do not see any indications to that fact in the photoelectron spectrum. Therefore, if the $^1A_1$ state is a transition state, it must be in a region of the potential energy surface that is exceptionally flat. In addition to the peaks listed in Table 2, we also find weak, unresolved signal in the region of 1.3–2.0 eV. The amount of signal in this region depends on the temperature of the ions, in that the signal is more intense if the experiments are carried out at room temperature. This suggests that some or all of the signal is due to transitions from excited vibrational states of the ion (vide infra). It is also possible that some of the signal comes from formation of the $\tilde{a}$ $^1B_1$ state, but is too weak to be assigned.

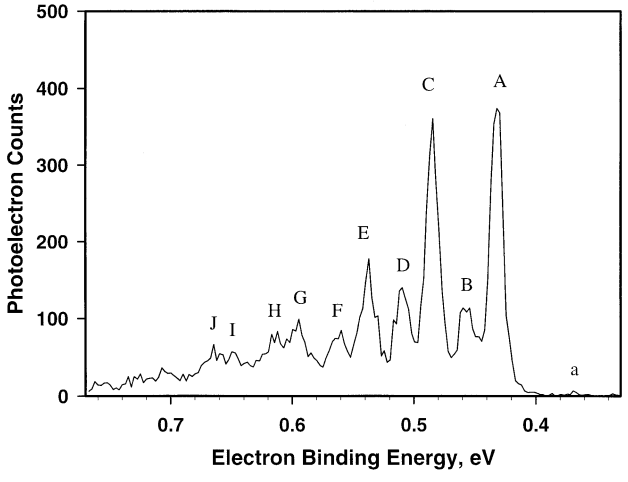

Figure 5. Expanded view of the triplet region of the photoelectron spectrum. Positions of the peaks labeled A–J are listed in Table 2.

Gas-Phase Acidity

The proton affinity of TMM^- (or, conversely, ΔH_{acid}(2-MeAllyl)) was determined by combining the results of two different approaches. Proton affinities of radical anions such as TMM^- are typically obtained by bracketing [85]. For example, TMM^- is observed to undergo proton transfer reaction with D_2O (ΔH_{acid} = 392.9 ± 0.1 kcal/mol) [86] and ethylmethylamine (ΔH_{acid} = 395.1 ± 2.1 kcal/mol) [86] but not with dimethylamine (ΔH_{acid} = 396.4 ± 0.7 kcal/mol) [86]. This suggests that the proton affinity of TMM^- is between 395.1 and 396.4 kcal/mol. However, interpretation of the bracketing results is complicated by the presence of competing reactions, e.g., hydrogen atom transfer, that occur between TMM^- and the reference acid amines. Therefore, the gas-phase acidity of 2-methylallyl radical was also determined by measuring the threshold energy for the

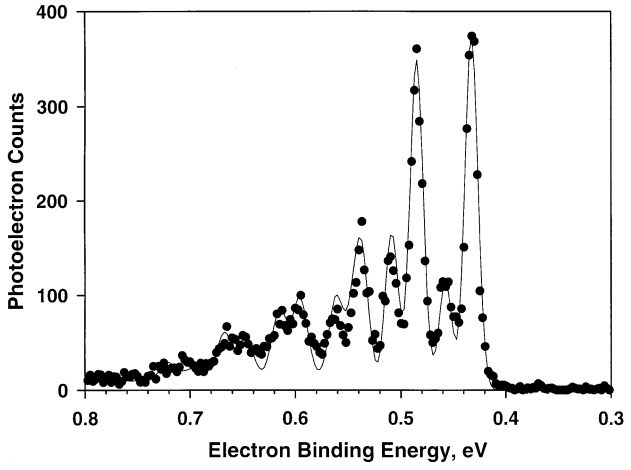

Figure 6. Franck–Condon fit of the triplet region of the photoelectron spectrum. The data are shown as solid circles, and the calculated fit is shown as the solid line.

proton transfer reaction between TMM^- and ammonia. The procedure for measuring the proton affinity is similar to that described by Chyall and Squires [87] in their study of the thermochemical properties of cyclopropenylidene, and involves monitoring the yield of proton transfer product (NH_2^-) as a function of the translational energy of the reactant ion. A typical appearance curve for the formation of NH_2^- in the reaction of TMM^- with NH_3 and the empirical fit to the data are shown in Figure 7. The threshold energy measured for the reaction of TMM^- and ammonia ($\Delta H_{acid}(NH_3)$ = 404.0 ± 0.4 kcal/mol) [85] is 0.48 ± 0.08 eV (11.0 ± 1.8 kcal/mol), where the uncertainty is four times the standard deviation of replicate measurements, and n = 1.61 (eq 3). Assuming that the temperature dependence is negligible, this gives ΔH_{acid}(2-MeAllyl) = 393.0 ± 1.8 kcal/mol, slightly lower than the value obtained from the bracketing experiments described above. The gas-phase acidity that we use for 2-methylallyl radical in this work is 394 ± 2 kcal/mol. This value includes the results from both the bracketing results and from the threshold measurements. In addition, it is also consistent with the observation that TMM^- reacts with amines by hydrogen atom transfer. In order for this reaction to occur, the proton affinity of TMM^- must be greater than 393.5 ± 2.0 kcal/mol.

Discussion

In this section, we discuss the important aspects of the photoelectron spectrum of TMM^-. Among the features to be addressed are the vibrational structure and the thermochemical properties. However, we begin by discussing the singlet–triplet splitting in TMM.

Singlet–Triplet Splitting

The measured energy difference between the $\tilde{X}\ ^3A_2'$ and $\tilde{b}\ ^1A_1$ states in TMM is 16.1 ± 0.1 kcal/mol, as determined from the positions of the origin peaks in the two features. This is the singlet–triplet energy difference in *planar* TMM and is within the range predicted by ab initio molecular orbital calculations. The $\tilde{X}\ ^3A_2' - \tilde{a}\ ^1B_1$ energy difference cannot be determined directly from the photoelectron spectrum. However, the most reliable molecular orbital calculations [58, 60, 61, 64–66] predict that the $\tilde{a}\ ^1B_1$ state is 0–3 kcal/mol more stable than the $\tilde{b}\ ^1A_1$ state, which suggests that the energy difference between the $^3A_2'$ and $^1A_1$ states is 13–16 kcal/mol.

This estimate of the singlet–triplet splitting in TMM is 6–9 kcal/mol higher than the value of 7 kcal/mol proffered on the basis of the rate of disappearance of the signal in the EPR spectrum [68]. The reason for the apparently low value for the singlet–triplet splitting obtained by Dowd and Chow has been the subject of numerous previous studies [59, 60, 62, 67], and remains unsolved. The discrepancy between our measured singlet–triplet splitting and that obtained by Dowd and Chow indicates that either the energy difference between the $^1B_1$ and $^1A_1$ states is larger than the 0–3 kcal/mol predicted by the calculations, or that the activation energy measured in the EPR experiments is not the singlet–triplet splitting in TMM.

Enthalpy of Formation of TMM

The enthalpy of formation of TMM can be calculated using eq 4,

$$\begin{aligned}\Delta H_{f,298}(\text{TMM}) = {} & \text{EA(TMM)} + \Delta H_{acid}(\text{2-MeAllyl}) \\ & + \text{EA(2-MeAllyl)} \\ & + \Delta H_{acid}(Me_2C{=}CH_2) \\ & + \Delta H_{f,298}(Me_2C{=}CH_2) \\ & - DH_{298}(H_2) - 2\text{IP(H)} \end{aligned} \quad (4)$$

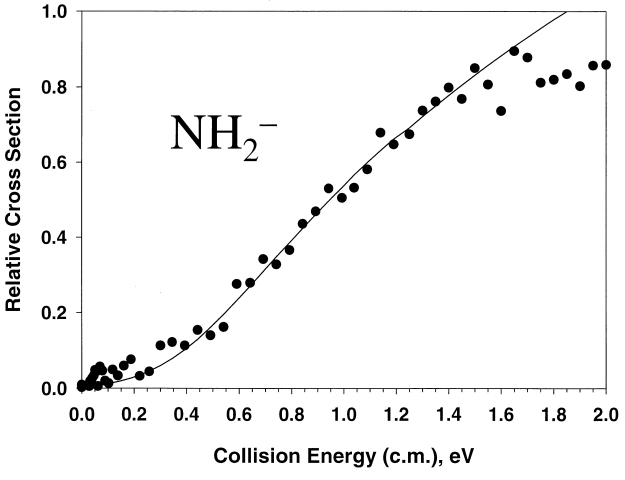

Figure 7. Relative cross sections for the formation of NH_2^- as a function of center-of-mass collision energy for the proton transfer reaction of TMM^- with NH_3. The solid line is the fully convoluted appearance curve obtained using the model given by eq 3.

where EA(TMM) and EA(2-MeAllyl) refer to the electron affinities of TMM and 2-methylallyl radical, respectively, $\Delta H_{acid}(Me_2C = CH_2)$ and ΔH_{acid}(2-MeAllyl) are the 298-K gas-phase acidities of 2-methylpropene and 2-methylallyl radical, respectively. These values are 390.3 ± 2.3 [86] and 394 ± 3 kcal/mol (vide supra), respectively. The remaining data are taken from the literature [88]. The electron affinity of 2-methylallyl radical was measured recently using negative ion photoelectron spectroscopy [12]. Using EA(2-MeAllyl) = 0.505 ± 0.006 eV in eq 4 leads to a value of 70 ± 3 kcal/mol for the enthalpy of formation of TMM, which agrees with an "additivity" value of 68.3 ± 3.3 kcal/mol derived using the enthalpy of formation and carbon–hydrogen bond energy of 2-methylpropene [12]. Molecular orbital calculations agree that the enthalpy of formation of TMM should be near that of bond additivity [38, 89].

The C–H bond enthalpy of 2-methylallyl radical can be calculated using eq 5 [85], where the temperature correction term has been neglected.

$$DH_{298}(\text{2-MeAllyl}) = \Delta H_{acid}(\text{2-MeAllyl}) + \text{EA(TMM)} - \text{IP(H)} \qquad (5)$$

From the data measured here, DH_{298}(2-MeAllyl) is calculated to be 90 ± 2 kcal/mol. This is similar to the C–H bond enthalpy in isobutene, 88.3 ± 2.3 kcal/mol, and is consistent with the value predicted by simple bond promotion energy models [90, 91].

Vibrational Assignments

In this section, we discuss the vibrational structure observed in the photoelectron spectra, and assign the vibrational modes by comparing to the previously reported vibrational frequencies, the photoelectron spectra of similar ions, and molecular orbital calculations.

The analysis begins with the vibrational structure observed for the ground state. For the triplet state we observe directly vibrational frequencies of 200, 425, 1310, and 1455 cm^{-1}. Moreover, an additional mode of 915 cm^{-1} is required in order to model the spectrum accurately. Some of these vibrational modes can be readily assigned by comparison with the photoelectron spectrum of allyl anion [12]. In that spectrum, vibrational frequencies of 425 and 990 cm^{-1} were observed and assigned to CCC bending and CCC stretching, respectively. We can assign the observed 425 and 915 cm^{-1} frequencies to corresponding modes in TMM. The 425-cm^{-1} mode is an E′ mode in D_{3h} TMM, corresponding to CCC bending. This mode is active because the ion has a C_{2v} geometry due to Jahn–Teller distortion. The mode at 915 cm^{-1} corresponds to the symmetric CC stretching mode in TMM.

In the spectrum of allyl anion, we observed a peak at 1600 cm^{-1}, an overtone of the 800-cm^{-1} CH_2 out-of-plane bending mode that is the most intense peak in the IR spectrum [52, 53]. Corresponding peaks are expected in the spectrum of TMM^-, and the 1310- and 1455-cm^{-1} modes are possible candidates. On the basis of molecular orbital calculations [53, 92], we assign the 1310-cm^{-1} frequency to stretching of a single C–C bond, which couples the C_{2v} structure of the ion with the D_{3h} structure of the triplet. This then leaves the mode at 1455 cm^{-1} as a likely overtone ($v = 2$) of an asymmetric mode in TMM. This is in fair agreement with the value of 1511 cm^{-1} obtained by doubling the A_2'' frequency that is the main peak in the IR spectrum of TMM as obtained by Maier and co-workers [52, 53]. The situation is slightly more complex because Maier et al. [53] also observed a peak at 1455 cm^{-1} in the IR spectrum of TMM, and assigned it to a combination band. However, this combination band is not likely to be intense in the photoelectron spectrum. Moreover, the transition that we observe has an intensity relative to the fundamental which is completely consistent with a simple Franck–Condon progression, further buttressing our assignment. Maier and co-workers also report a value of 1418.4 cm^{-1} for the e′ CH_2 scissoring mode [52, 53] that is not observed in the photoelectron spectrum.

The only frequency left to assign is the apparent mode at 200 cm^{-1}. Vibrational frequencies calculated for triplet TMM do not include any values this low [53, 92], as the CCC bending e′ mode at 425 cm^{-1} is calculated to be the lowest frequency vibration. Most likely, the peak at 200 cm^{-1} is a sequence band that arises from $v = 1$ in an asymmetric mode in the ion to $v = 1$ in the neutral. In order to see this type of transition at this energy, the frequency in the neutral must be 200 cm^{-1} higher than that for the corresponding mode in the ion. Moreover, the ion frequency must be sufficiently low in energy to be populated at the 200-K temperature of the ion. We have identified vibrational modes in the molecular orbital calculations that may satisfy these criteria. At the B3LYP/aug-cc-pVDZ level of theory, the $^2A_2$ ion has a b_2 mode at 280 cm^{-1} that corresponds to the 425-cm^{-1} e′ mode observed in the spectrum. This vibration consists of in-plane distortion of the carbon framework. The ion frequency is sufficiently low for excited states to be populated at 200 K (~12% in $v = 1$), and the calculated frequency difference is reasonably close to the measured value. There is a second mode, which consists of conrotary twisting of the three methylene groups that has a calculated frequency of 308 cm^{-1} in the ion and 478 cm^{-1} in the triplet, a difference of 170 cm^{-1}. This is also in reasonable agreement with what is observed in the spectrum. However, although $v = 1$ for 308 cm^{-1} mode will be populated at 200 K, it will not be to the same extent as that for the 270-cm^{-1} vibration. Given the accuracy of the calculations for frequencies of this magnitude, either of these transitions could give rise to the 200-cm^{-1} progression in the spectrum of TMM^-.

Assignments of the vibrational modes in the $^1A_1$ state of TMM are more difficult than for the triplet state

because none of the vibrational frequencies in this state are presently known and they are difficult to calculate. Two progressions are observed in the $^1A_1$ region of the TMM^- photoelectron spectrum, at 90 and 335 cm^{-1}. The 335-cm^{-1} mode most likely corresponds to CCC bending that is active in the triplet state, while the 90-cm^{-1} mode is likely the same type of sequence band that was observed for the triplet state.

Conclusions

The physical properties reported for TMM from this work, the electron affinity, enthalpy of formation, singlet–triplet splitting, and vibrational frequencies, compliment the experimental data previously reported by investigators such as Dowd [39], Berson [40], and Maier [53], and their co-workers, and the theoretical studies of Schaefer [60, 65, 92], Borden [41], and others [58, 61]. The ability to carry out the work in the gas phase allows for straightforward interpretation of the data obtained, and illustrates the contributions that mass spectrometric approaches can make in this field. However, even with all the information that has been obtained from these experiments, important, outstanding problems still remain. Therefore, additional studies are required for this challenging biradical.

Acknowledgments

We are very pleased to acknowledge the support of this work by the National Science Foundation (W.C.L.: CHE97-03486 and PHY95-12150; R.R.S.: CHE97-32696).

References

1. Rosenstock, H. M.; Stockbauer, R.; Parr, A. C. *J. Chim. Phys.* **1980,** *77*, 745.
2. Pollack, S. K.; Hehre, W. J. *Tetrahedron Lett.* **1980,** *21*, 2483.
3. Maccoll, A.; Mathur, D. *Org. Mass Spectrom.* **1981,** *16*, 261.
4. Moini, M.; Leroi, G. E. *J. Phys. Chem.* **1986,** *90*, 4002.
5. Riveros, J. M.; Ingemann, S.; Nibbering, N. M. M. *J. Am. Chem. Soc.* **1991,** *113*, 1053.
6. Guo, Y.; Grabowski, J. J. *J. Am. Chem. Soc.* **1991,** *113*, 5923.
7. Wenthold, P. G.; Squires, R. R. *J. Am. Chem. Soc.* **1994,** *116*, 6401.
8. Matimba, H. E. K.; Crabbendam, A. M.; Ingemann, S.; Nibbering, N. M. M. *J. Chem. Soc., Chem. Commun.* **1991,** *9*, 644.
9. Gunion, R. F.; Gilles, M. K.; Polak, M. L.; Lineberger, W. C. *Int. J. Mass Spectrom. Ion Processes* **1992,** *117*, 601.
10. Robinson, M. S.; Polak, M. L.; Bierbaum, V. M.; DePuy, C. H.; Lineberger, W. C. *J. Am. Chem. Soc.* **1995,** *117*, 6766.
11. Gunion, R. F.; Karney, W.; Wenthold, P. G.; Borden, W. T.; Lineberger, W. C. *J. Am. Chem. Soc.* **1996,** *118*, 5074.
12. Wenthold, P. G.; Polak, M. L.; Lineberger, W. C. *J. Phys. Chem.* **1996,** *100*, 6920.
13. Kato, S.; Lee, H. S.; Gareyev, R.; Wenthold, P. G.; Lineberger, W. C.; DePuy, C. H.; Bierbaum, V. M. *J. Am. Chem. Soc.* **1997,** *119*, 7863.
14. Burnett, S. M.; Stevens, A. E.; Feigerle, C. S.; Lineberger, W. C. *Chem. Phys. Lett.* **1983,** *100*, 124.
15. Murray, K. K.; Leopold, D. G.; Miller, T. M.; Lineberger, W. C. *J. Chem. Phys.* **1988,** *89*, 5442.
16. Ervin, K. M.; Ho, J.; Lineberger, W. C. *J. Chem. Phys.* **1989,** *91*, 5974.
17. Gilles, M. K.; Ervin, K. M.; Ho, J.; Lineberger, W. C. *J. Phys. Chem.* **1992,** *96*, 1130.
18. Gilles, M. K.; Lineberger, W. C.; Ervin, K. M. *J. Am. Chem. Soc.* **1993,** *115*, 1031.
19. Gunion, R. F.; Köppel, H.; Leach, G. W.; Lineberger, W. C. *J. Chem. Phys.* **1995,** *103*, 1250.
20. Gunion, R. F.; Lineberger, W. C. *J. Phys. Chem.* **1996,** *100*, 4395.
21. Leopold, D. G.; Stevens-Miller, A. E.; Lineberger, W. C. *J. Am. Chem. Soc.* **1986,** *108*, 1379.
22. Wenthold, P. G.; Kim, J. B.; Lineberger, W. C. *J. Am. Chem. Soc.* **1997,** *119*, 1354.
23. Wenthold, P. G.; Squires, R. R.; Lineberger, W. C. *J. Am. Chem. Soc.* **1998,** *120*, 5279.
24. Wenthold, P. G.; Lineberger, W. C. *J. Am. Chem. Soc.* **1997,** *119*, 7772.
25. Wenthold, P. G.; Hrovat, D.; Borden, W. T.; Lineberger, W. C. *Science* **1996,** *272*, 1456.
26. Dowd, P. *J. Am. Chem. Soc.* **1970,** *92*, 1066.
27. Dowd, P.; Chang, W.; Paik, Y. H. *J. Am. Chem. Soc.* **1986,** *108*, 7416.
28. Berson, J. A. *Acc. Chem. Res.* **1997,** *30*, 238.
29. Du, P.; Borden, W. T. *J. Am. Chem. Soc.* **1987,** *109*, 930.
30. Du, P.; Borden, W. T. *J. Am. Chem. Soc.* **1992,** *114*, 4949.
31. Borden, W. T.; Iwamura, H.; Berson, J. A. *Acc. Chem. Res.* **1994,** *27*, 109.
32. Choi, Y.; Jordan, K. D.; Paik, Y. H.; Chang, W.; Dowd, P. *J. Am. Chem. Soc.* **1988,** *110*, 7575.
33. Nachtigall, P.; Dowd, P.; Jordan, K. D. *J. Am. Chem. Soc.* **1992,** *114*, 4747.
34. Nachtigall, P.; Jordan, K. D. *J. Am. Chem. Soc.* **1992,** *114*, 4743.
35. Nachtigall, P.; Jordan, K. D. *J. Am. Chem. Soc.* **1993,** *115*, 270.
36. Nash, J. J.; Dowd, P.; Jordan, K. D. *J. Am. Chem. Soc.* **1992,** *114*, 10071.
37. Clifford, E. P.; Wenthold, P. G.; Lineberger, W. C.; Ellison, G. B.; Wang, C. X.; Grabowski, J. J.; Vila, F.; Jordan, K. D. *J. Chem. Soc., Perkin Trans. 2* **1998,** *005*, 1015.
38. Wenthold, P. G.; Hu, J.; Squires, R. R.; Lineberger, W. C. *J. Am. Chem. Soc.* **1996,** *118*, 475.
39. Dowd, P. *Acc. Chem. Res.* **1972,** *5*, 242.
40. Berson, J. *Acc. Chem. Res.* **1978,** *11*, 446.
41. Borden, W. T.; Davidson, E. R. *Acc. Chem. Res.* **1981,** *14*, 69.
42. Weiss, F. *Q. Rev. Chem. Soc.* **1970,** *24*, 278.
43. Coulson, C. A. *J. Chim. Phys.* **1948,** *45*, 243.
44. Doering, W. V. E.; Roth, H. D. *Tetrahedron* **1970,** *26*, 2825.
45. Gajewski, J. J. *Hydrocarbon Thermal Isomerizations*; Academic: New York, 1981.
46. Borden, W. T. In *Diradicals*; Borden, W. T., Ed.; Wiley: New York, 1982; p 1.
47. Dowd, P. *J. Am. Chem. Soc.* **1966,** *88*, 2587.
48. Dowd, P.; Sachdev, K. *J. Am. Chem. Soc.* **1967,** *89*, 715.
49. Dowd, P.; Gold, A.; Sachdev, K. *J. Am. Chem. Soc.* **1968,** *90*, 2715.
50. Baseman, R. J.; Pratt, D. W.; Chow, M.; Dowd, P. *J. Am. Chem. Soc.* **1976,** *98*, 5726.
51. Berson, J. In *Diradicals*; Borden, W. T., Ed.; Wiley: New York, 1982; p 151.
52. Maier, G.; Reisenauer, H. P.; Lanz, K.; Tross, R.; Jürgen, D.; Hess, Jr., B. A.; Schaad, L. J. *Angew. Chem., Int. Ed. Eng.* **1993,** *32*, 74.
53. Maier, G.; Jürgen, D.; Tross, R.; Reisenauer, H. P.; Hess, Jr., B. A.; Schaad, L. J. *Chem. Phys.* **1994,** *189*, 367.
54. Jacobs, S. J.; Schultz, D. A.; Jain, R.; Novak, J.; Dougherty, D. A. *J. Am. Chem. Soc.* **1993,** *115*, 1744.
55. Trost, B. M. *Angew. Chem. Int. Ed., Eng.* **1986,** *25*, 1.

56. Bregant, T. M.; Groppe, J.; Little, R. D. *J. Am. Chem. Soc.* **1994,** *116*, 3635.
57. Borden, W. T.; Davidson, E. R. *J. Am. Chem. Soc.* **1977,** *99*, 4587.
58. Davis, J. H.; Goddard III, W. A. *J. Am. Chem. Soc.* **1977,** *99*, 4242.
59. Dixon, D. A.; Foster, R.; Halgren, T. A.; Lipscomb, W. N. *J. Am. Chem. Soc.* **1978,** *100*, 1359.
60. Ma, B.; Schaefer III, H. F. *Chem. Phys.* **1996,** *207*, 31.
61. Cramer, C. J.; Smith, B. A. *J. Phys. Chem.* **1996,** *100*, 9664 and references therein.
62. Feller, D.; Tanaka, K.; Davidson, E. R.; Borden, W. T. *J. Am. Chem. Soc.* **1982,** *104*, 967.
63. Lewis, S. B.; Hrovat, D. A.; Getty, S. J.; Borden, W. T., unpublished.
64. Yarkony, D. R.; Schaefer III, H. F. *J. Am. Chem. Soc.* **1974,** *96*, 3754.
65. Hood, D. M.; Pitzer, R. M.; Schaefer III, H. F. *J. Am. Chem. Soc.* **1978,** *100*, 2227.
66. Auster, S. B.; Pitzer, R. M.; Platz, M. S. *J. Am. Chem. Soc.* **1982,** *104*, 3812.
67. Skancke, A.; Schaad, L. J.; Hess Jr., B. A. *J. Am. Chem. Soc.* **1988,** *110*, 5315.
68. Dowd, P.; Chow, M. *J. Am. Chem. Soc.* **1977,** *99*, 6438.
69. Hehre, W. J.; Salem, L.; Willcott, M. R. *J. Am. Chem. Soc.* **1974,** *96*, 4328.
70. Ollivella, S.; J. *Int. J. Quant. Chem.* **1990,** *37*, 713.
71. Lee, J.; Grabowski, J. J. *Chem. Rev.* **1992,** *92*, 1611.
72. Bruins, A. P.; Ferrer-Correia, A. J.; Harrison, A. G.; Jennings, K. R.; Mitchum, R. K. *Adv. Mass. Spectrom.* **1978,** *7*, 355.
73. Zhao, J.; Dowd, P.; Grabowski, J. J. *J. Am. Chem. Soc.* **1996,** *118*, 8871.
74. Wenthold, P. G.; Hu, J.; Hill, B. T.; Squires, R. R. *Int. J. Mass Spectrom.* **1998,** *179/180*, 173.
75. Wenthold, P. G.; Hu, J.; Squires, R. R. *J. Am. Chem. Soc.* **1994,** *116*, 6961.
76. Ervin, K. M.; Lineberger, W. C. In *Advances in Gas Phase Ion Chemistry*; Adams, N. G.; Babcock, L. M., Eds.; JAI Press: Greenwich, 1992; Vol 1; p 121.
77. Neumark, D. M.; Lykke, K. R.; Andersen, T.; Lineberger, W. C. *Phys. Rev. A* **1985,** *32*, 1890.
78. Moore, C. E. Atomic Energy Levels; US GPO Circular No. 467: Washington, 1952.
79. Marinelli, P. J.; Paulino, J. A.; Sunderlin, L. S.; Wenthold, P. G.; Poutsma, J. C.; Squires, R. R. *Int. J. Mass Spectrom. Ion Processes* **1994,** *130*, 89.
80. Armentrout, P. B. In *Advances in Gas Phase Ion Chemistry*; Adams, N. G.; Babcock, L. M., Eds.; JAI: Greenwich, CT, 1992; Vol 1.
81. Chantry, P. J. *J. Chem. Phys.* **1971,** *55*, 2746.
82. Nash, J. J.; Squires, R. R. *J. Am. Chem. Soc.* **1996,** *118*, 11872.
83. Duschinsky, F. *Acta Physicochim. URSS* **1937,** *7*, 551.
84. Neumark, D. M. *Acc. Chem. Res.* **1993,** *26*, 33.
85. Berkowitz, J.; Ellison, G. B.; Gutman, D. *J. Phys. Chem.* **1994,** *98*, 2744.
86. Bartmess, J. E. In *NIST Chemistry WebBook, NIST Standard Reference Database Number 69*; Mallard, W. G.; Lindstrom, P. J., Eds.; National Institute of Standards and Technology: Gathersburg, MD, 1998 (http://webbook.nist.gov).
87. Chyall, L. J.; Squires, R. R. *Int. J. Mass Spectrom. Ion Processes* **1995,** *149/150*, 257.
88. Pedley, J. B.; Naylor, R. D.; Kirby, S. P. *Thermochemistry of Organic Compounds*, 2nd ed.; Chapman and Hall: New York, 1986.
89. Getty, S. J.; Hrovat, D. A.; Xu, J. D.; Barker, S. A.; Borden, W. T. *J. Chem. Soc., Faraday Trans.* **1994,** *90*, 1689.
90. Clauberg, H.; Minsek, D. W.; Chen, P. *J. Am. Chem. Soc.* **1992,** *114*, 99.
91. Zhang, X.; Chen, P. *J. Am. Chem. Soc.* **1992,** *114*, 3147.
92. Blahous III, C. P.; Xie, Y.; Schaefer III, H. F. *J. Chem. Phys.* **1990,** *92*, 1174.